Asymmetric band gaps in a Rashba film system

C. Carbone,[1,][*] P. Moras,[1] P. M. Sheverdyaeva,[1] D. Pacilé,[1,2] M. Papagno,[1,2] L. Ferrari,[3] D. Topwal,[4,5] E. Vescovo,[6]
G. Bihlmayer,[7] F. Freimuth,[7] Y. Mokrousov,[7] and S. Blügel[7]

[1]*Istituto di Struttura della Materia, Consiglio Nazionale delle Ricerche, I-34149 Trieste, Italy*
[2]*Dipartimento di Fisica, Università della Calabria, I-87030 Arcavacata di Rende, Italy*
[3]*Istituto dei Sistemi Complessi, Consiglio Nazionale delle Ricerche, I-00185 Roma, Italy*
[4]*International Centre for Theoretical Physics, I-34151 Trieste, Italy*
[5]*Institute of Physics, Sachivalaya Marg, Bhubaneswar 751005, India*
[6]*National Synchrotron Light Source, Brookhaven National Laboratory, Upton, New York 11973, USA*
[7]*Peter Grünberg Institut and Institute for Advanced Simulation, Forschungszentrum Jülich and JARA, D-52425 Jülich, Germany*

The joint effect of exchange and Rashba spin-orbit interactions is examined on the surface and quantum well states of Ag_2Bi-terminated Ag films grown on ferromagnetic Fe(110). The system displays a particular combination of time-reversal and translational symmetry breaking that strongly influences its electronic structure. Angle-resolved photoemission reveals asymmetric band-gap openings, due to spin-selective hybridization between Rashba-split surface states and exchange-split quantum well states. This results in an unequal number of states along positive and negative reciprocal space directions. We suggest that the peculiar asymmetry of the discovered electronic structure can have significant influence on spin-polarized transport properties.

I. INTRODUCTION

Some of the most exciting prospects in spintronics reside in the area of spin-orbit interaction driven phenomena, which manifest prominently at surfaces and interfaces of topological insulators and Rashba systems [1–3]. The Rashba effect originates from the breaking of the translational symmetry of a crystalline material, which results in an effective electric potential gradient, seen in the rest-frame of the electron as a magnetic field perpendicular to the in-plane wave vector **k** [4,5]. This field lifts the spin degeneracy of the electrons moving in the surface plane and causes a band splitting. Due to the lack of structural inversion symmetry, the electronic states have to satisfy the relation $E_{\uparrow\downarrow,\mathbf{k}} = E_{\downarrow\uparrow,-\mathbf{k}}$ rather than $E_{\uparrow\downarrow,\mathbf{k}} = E_{\uparrow\downarrow,-\mathbf{k}}$ as in a centrosymmetric crystal structure.

The Rashba effect is well known for narrow-gap 2DEG semiconductors [6], hybrid systems [3], as well as metallic systems [7,8]. For heavy elements, such as Au and Bi, the Rashba spin-orbit interaction results in well-separated spin-polarized surface bands, split by a few hundred meV. Similarly, a giant Rashba effect occurs in substitutional Ag_2X/Ag(111) surface alloys (X = Pb, Bi), where the Rashba splitting is significantly enhanced with respect to the one of the pure Ag surface [9].

The Rashba spin-orbit interaction gives rise to spin-momentum locking due to a correlation between the **k** vector and the direction of the local spin quantization axis (SQA) in reciprocal space. Analogously to the case of topological insulators, the complex relationship between **k** and spin of Rashba states exposed to an exchange field, provides intriguing scenarios with novel perspectives for transport, which sensitively depend on the relative strength of the exchange splitting and spin-orbit interaction. For example,

Dirac bands subjected to Rashba spin-orbit and exchange interactions exhibit the quantum anomalous Hall effect [10]. On the other hand, current-induced spin-orbit effective magnetic fields, originating from the Rashba effect at the interface between a ferromagnet and a paramagnet [11–14], have been recently experimentally observed to promote domain motion and magnetization switching in metal films [15,16] and dilute magnetic semiconductors [17,18].

Overall, there is an essential need for microscopic understanding and insights into material design of Rashba states brought in contact with magnetization or exchange field. Until now, the only direct observations of the Rashba effect in magnetic systems relate to a spin-polarized surface band of pristine and oxidized rare-earth metals [19], films of Co on W(110) [20] and Ni surfaces [21], displaying a small **k** shift upon magnetization reversal.

In this work we examine the interplay of exchange and spin-orbit Rashba interactions in a film system specifically designed with the aim to shed light on and emphasize their mutual effect. We report on the unusual behavior of the surface and quantum well states (QWS) of a thin Ag film, grown on Fe(110), whose surface Rashba effect is enhanced by Bi alloying. The whole band structure of the film acquires, as a joint result of Rashba and exchange interactions, a dependence on the magnetization direction. In particular, the concurrent lack of inversion and time reversal symmetry gives rise to asymmetric gap openings, in addition to a very pronounced **k** vs −**k** asymmetry of the band dispersion. The data are analyzed on the basis of density functional theory (DFT) calculations. Model transport calculations reveal important implications of such asymmetries for spin-polarized transport and magnetization manipulation.

II. EXPERIMENTAL AND COMPUTATIONAL DETAILS

Angle-resolved photoemission spectra were measured at the VUV-photoemission beamline of the Elettra synchrotron.

————
[*]carlo.carbone@trieste.ism.cnr.it

Epitaxial film structures were produced *in situ*, through a sequence of growth steps, which individually followed established preparation procedures. A W(110) crystal was used to grow epitaxial Fe(110) films. Atomically flat Ag(111) films were grown on the Fe(110) surface, with crystallographic relations Ag [$1\bar{1}0$]‖ Fe [001] and Ag [$11\bar{2}$]‖ Fe [$1\bar{1}0$]. Finally, a ($\sqrt{3} \times \sqrt{3}$)$R30°$ Ag_2Bi alloy was produced on the Ag surface by deposition of one-third Bi monolayer (ML). Sharp low energy electron diffraction patterns were observed at all growth stages. The Fe films were remanently magnetized along the Fe [001] (M^+) or the Fe [$00\bar{1}$] (M^-) direction (see Appendix A).

We analyze the film band structure by DFT calculations using the generalized gradient approximation [22] to the exchange correlation potential. Employing the full-potential linearized augmented plane-wave method [23,24] as implemented in the FLEUR code [25], we set up films consisting of five Fe ML, nine Ag ML, and a Ag_2Bi surface layer. The in-plane unit cell is ($\sqrt{3} \times \sqrt{3}$)$R30°$ with the Ag lattice parameter and relaxations for the Ag_2Bi surface alloy [26]. The Fe was stretched to match the Ag epitaxially, keeping the Fe(110) interlayer distances. The magnetization is in the film plane, as in the experiment.

III. RESULTS AND DISCUSSION

Spin-resolved photoemission on Ag(111) films grown on Fe(110) shows that the QWS resulting from electron confinement in the potential well defined by the vacuum and the Ag/Fe interface, display a spin-polarized character (see Appendix B and [27]). The exchange-split QWS are predominantly minority-spin polarized, because the Ag/Fe interface more effectively reflects minority-spin than majority-spin electrons. Majority-spin QWS are less confined in the Ag layer and are split by a few hundreds meV to higher binding energy (see Appendix B). Although the QWS spin polarization depends on the Fe magnetization direction and reverses its sign correspondingly, the QWS preserve the usual $E_{\uparrow\downarrow,\mathbf{k}} = E_{\uparrow\downarrow,-\mathbf{k}}$ relation.

This picture can change drastically when the spin-polarized QWS of an Ag film interact with Rashba-split surface bands. The bands of the Ag_2Bi alloy, formed on a Ag(111) surface, display pairs of downward dispersing bands with giant Rashba splitting [9]. On Ag films, these bands open multiple hybridization gaps where they cross QWS [28–30]. In the absence of magnetic interactions the Ag_2Bi surface bands, as well as the overall band structure of the film, obey the Rashba symmetry relation $E_{\uparrow\downarrow,\mathbf{k}} = E_{\downarrow\uparrow,-\mathbf{k}}$. However, particular asymmetry properties can arise from spin-selective hybridization when the QWS interacting with the Rashba states are spin polarized, as schematically indicated in Fig. 1. Spin-selective hybridization should lead in such a case to asymmetric band-gap openings, and, for certain binding energies, to an unequal number of states along the $\mathbf{k}$ and $-\mathbf{k}$ axis. A related consequence is the creation of an asymmetric distribution of singular points, in correspondence to the edges of the spin-polarized bands. The unusual scenario presented by this system, originating from coexisting time-reversal and structural inversion symmetry breaking, turns out to be experimentally verified in our photoemission data.
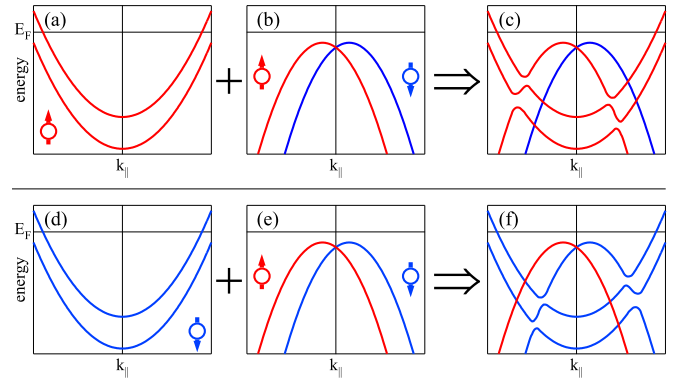

FIG. 1. Scheme of (a) and (d) spin-polarized QWS interacting with (b) and (e) Rashba-split surface states. Depending on the QWS spin orientation, spin-selective hybridization with the surface states results in (c) and (f) asymmetric ($\mathbf{k}$ vs $-\mathbf{k}$) band structures.

A. Angle-resolved photoemission

Angle-resolved photoemission spectra display the dispersion of sp-derived QWS for a 15-ML Ag(111) film on Fe(110), before [Figs. 2(a) and 2(d)] and after [Figs. 2(b) and 2(c)] the formation of the Ag_2Bi surface alloy. In this measurement geometry, along the $\overline{M} - \overline{\Gamma} - \overline{M}$ direction, the Fe magnetization defines a SQA of the QWS which is collinear with that of the Rashba surface states. The spin-selective hybridization between the downward-dispersing surface states and the upward-oriented QWS leads to two effects: The band structure becomes asymmetric for $\mathbf{k}$ and $-\mathbf{k}$, and acquires a dependence on the magnetization direction of the underlying Fe film [Figs. 2(b) and 2(c)]. The band dispersion and specifically the gap openings occurring where the QWS and the Rashba states interact, aside from the intensity variation due to the matrix element effects, display a marked asymmetry for positive and negative $\mathbf{k}$ vectors, which reverses with the sign of the Fe magnetization. This particular electronic character is clearly observed also in Figs. 2(e) and 2(f), which highlights how parts of the band structure change by reversing the Fe film magnetization.

Similar asymmetry effects are observed overall in $\mathbf{k}$ space, except for $\mathbf{k}$ vectors collinear with the magnetization direction, i.e., where the SQA of QWS and Rashba states are perpendicular to each other. Figure 3 shows photoemission spectra measured with a photon energy (28 eV) that enhances the Bi-related Rashba bands. The $\mathbf{k}$ vectors are perpendicular [Figs. 3(a) and 3(b)] and parallel [Figs. 3(d) and 3(e)] to the magnetization with the SQA of the QWS, respectively, parallel and perpendicular to the spin polarization of the Rashba states. A left-right band-gap asymmetry, depending on the Fe magnetization direction, is visible in Figs. 3(a) and 3(b), and vanishes in Figs. 3(d) and 3(e). Figures 3(c) and 3(f) summarize these asymmetry effects in the two geometries by reporting the spectral difference between the M^+ and M^- orientations.

A consequence of the asymmetric band-gap openings is that an unequal number of states is found on the positive and negative side of the k axis, for energies corresponding to a band gap. Figure 4 highlights this effect by showing a constant energy cut of the band structure of Ag_2Bi/11-ML

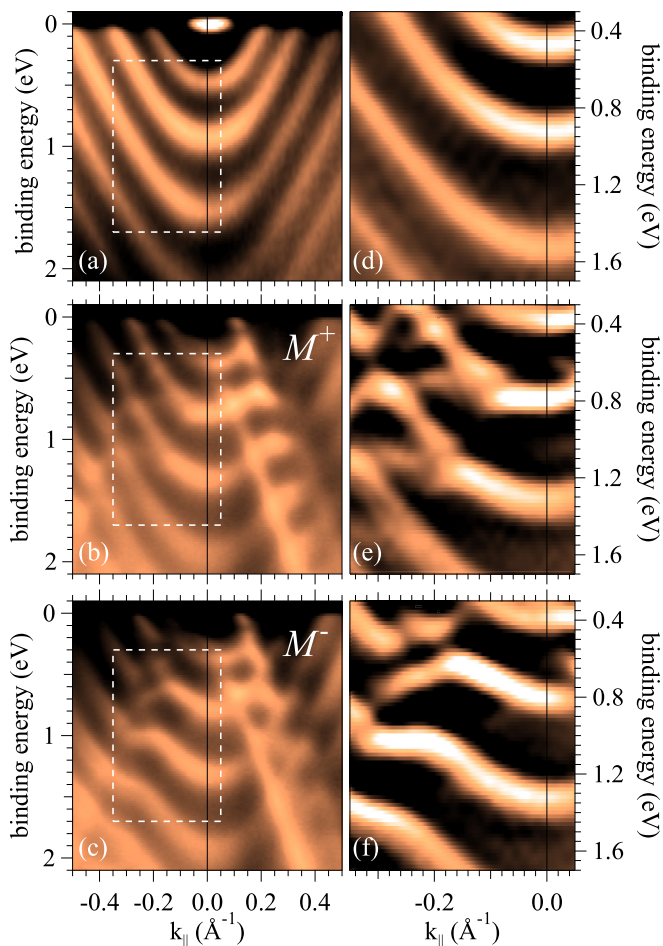FIG. 2. (a) Photoemission spectra for 15 ML Ag/Fe(110) along the $\overline{M} - \overline{\Gamma} - \overline{M}$ direction. (b) and (c) Photoemission spectra for Ag$_2$Bi/15 ML Ag/Fe(110) along $\overline{M} - \overline{\Gamma} - \overline{M}$ with collinear SQA of QWS and Rashba-split states, for opposite magnetization, M^+ and M^-, of the Fe film. (d)–(f) Second derivative spectra of the regions enclosed by the dashed lines in panels (a)–(c). The photon energy is 50 eV.

FIG. 3. Second derivative photoemission spectra of Ag$_2$Bi/15 ML Ag/Fe(110) with SQA of QWS *collinear* with Rashba states, measured with magnetization (a) M^+, (b) M^-, and (c) their difference. Second derivative photoemission spectra of Ag$_2$Bi/15 ML Ag/Fe(110) with SQA of QWS orthogonal to the Rashba states, for (d) M^+, (e) M^-, and (f) their difference.

Ag/Fe(110) film measured in correspondence of a gap opening. The presence of the band gap produces an arc with a half-moon shape, positioned either on the positive or negative **k** side, depending on the magnetization direction. For an energy exactly in the middle of the gap, and in optimal resolution condition, the curve would be reduced to a single state, i.e., to a singular point. Similar asymmetries are observed at other binding energies (see Appendix C), where band gaps occur. Such a particular band structure qualitatively differs from all other cases until now studied manifesting Rashba and exchange effect, in which the magnetization reversal results just in a *k* shift of a band [19–21].

B. Band structure calculations

The combined effect of the exchange and Rashba interaction, acting on the Ag film at the interface with ferromagnetic Fe and at the Bi-modified surface, respectively, was examined by DFT calculations. Figure 5 shows the film band structure, and the spin character of the Ag- and Bi-related states.
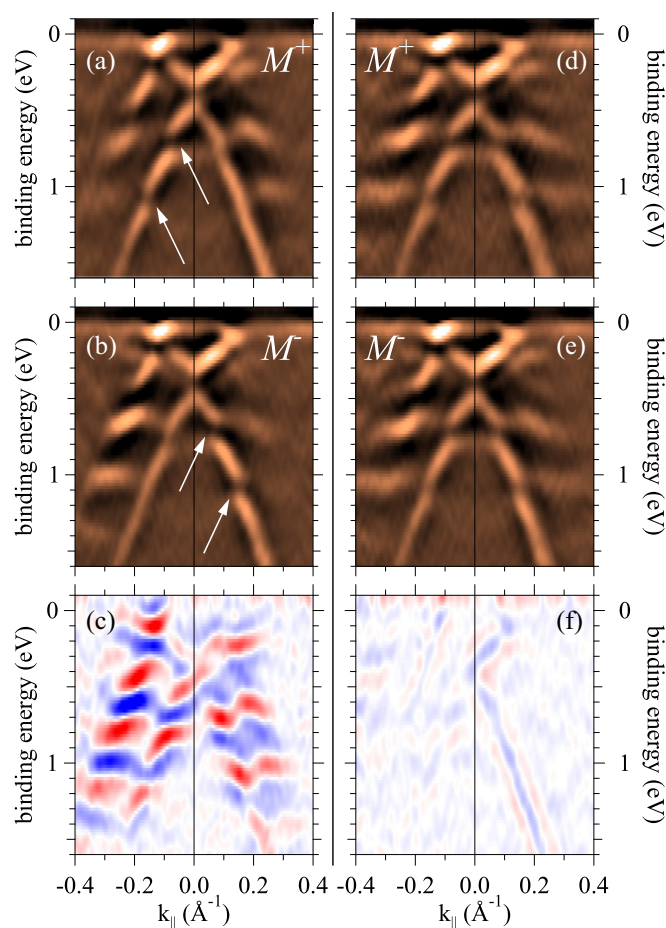
Although the induced spin polarization in the Ag film is negligibly small (about 0.01 μ_B at the interface, decaying to 0.0003 μ_B at the surface), the QWS show a sizable spin splitting, in the order of 0.4–0.5 eV. The size of the symbols in Fig. 5 indicates the localization of the wave function in the Ag film: The spin channel corresponding to the Fe minority-spin direction is better confined within the Ag layers (see Appendix B).

Turning to the crucial aspect of this investigation, the interaction of the QWS with the spin-orbit split Ag$_2$Bi alloy states, we first analyze the case of the Fe magnetization perpendicular to the electron propagation direction. Since the spin of the Ag$_2$Bi states is locked by the Rashba effect in the direction ($\mathbf{k} \times \mathbf{n}$), where **n** is the surface normal, the SQA of Ag$_2$Bi alloy states and Ag QWS coincide. The Rashba states and QWS of the same spin orientation hybridize and open gaps, while bands of opposite spin character are allowed to cross. This is particularly evident for the QWS originating at 2.0 eV at the $\overline{\Gamma}$ point. The next set of QWS, located at around 1.5 and 1.2 eV, exhibits smaller gap openings and smaller spin splitting when crossing the surface bands. The different spin splitting
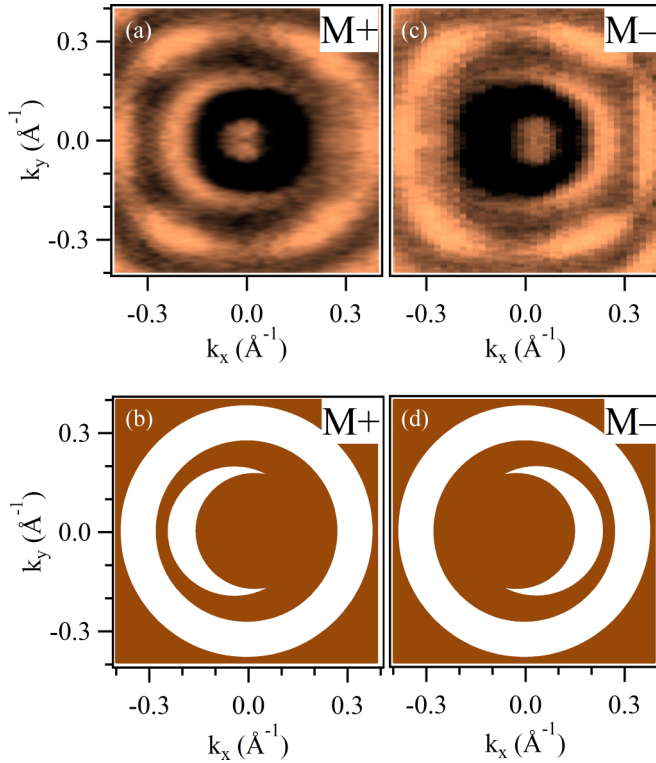
FIG. 4. Constant energy cut for the $Ag_2Bi/11$ ML Ag/Fe(110) film, taken at 0.54 eV binding energy with magnetization (a) M^+ and (c) M^- aligned along the vertical axis. (b) and (d) Schemes corresponding to (a) and (c). The photon energy is 50 eV.

of these states can be attributed to their degree of hybridization with Fe bands. The unusual asymmetry between the band structure for **k** and −**k** disappears for **k**-space directions for which the SQA of the QWS is parallel to the propagation direction of the electrons. In this case hybridization of the Ag_2Bi-related bands with QWS equally occurs for positive
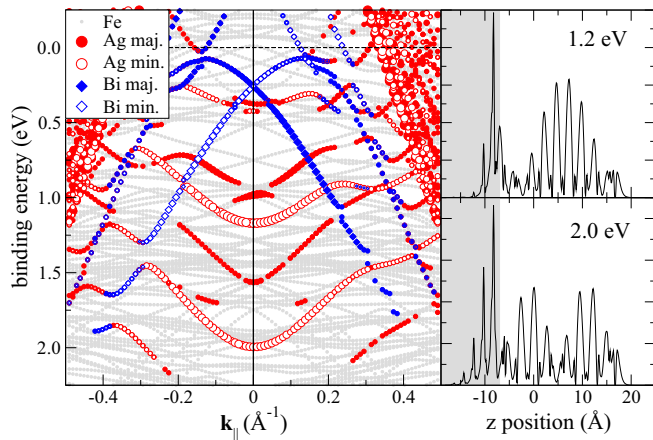
and negative **k**, as expected because the SQA of these states are now orthogonal to each other.

C. Model transport calculations

The most prominent consequence of the unusual **k** to −**k** asymmetry arises for spin-polarized transport properties of the film. Within linear response, the **k** vs −**k** asymmetry of the band structure is not visible in the conductivity. However, as shown below, the combination of anisotropic magnetoresistance (AMR) and current-induced spin polarization (CISP) allows one to observe this asymmetry in the quadratic response: For current perpendicular to the magnetization **M**, the CISP leads to an additional magnetization component δM that is either parallel or antiparallel to **M**, depending on the sign of the current, therefore the total magnetization $M + \delta M$ in the presence of a current is either smaller or larger than the equilibrium magnetization. Since the resistance depends also on the magnitude of **M**, this leads to a current-dependent resistivity, which can be observed as the quadratic term in the current-voltage characteristic.

To estimate the strength of these effects, we performed calculations that capture the essential properties of the electronic structure by 4×4 model Hamiltonian leading to a band structure displayed in Figs. 6(a) and 6(b) (see Appendix D). In agreement with the previous discussion, the **k** vs −**k** asymmetry is present if **k** is perpendicular to the magnetization [Fig. 6(b)] and absent if **k** is parallel to it [Fig. 6(a)]. Note that the in-plane asymmetry in this model is only due to the magnetization direction; for **M** in the z direction the Hamiltonian is rotational symmetric around the surface normal.

Next, we study the CISP and AMR for the above model in the diffusive regime, describing disorder by identical scalar point defects located at random positions. We use the Born approximation for the self-energy and treat the vertex corrections within the ladder approximation. It is known that in the Rashba model without exchange a spin polarization is generated in the presence of a current [2,31]. We expect the additional QWS in our model to significantly alter the CISP. The current induced spin density per current density, denoted by S, is plotted in Fig. 6(c) as a function of binding energy.
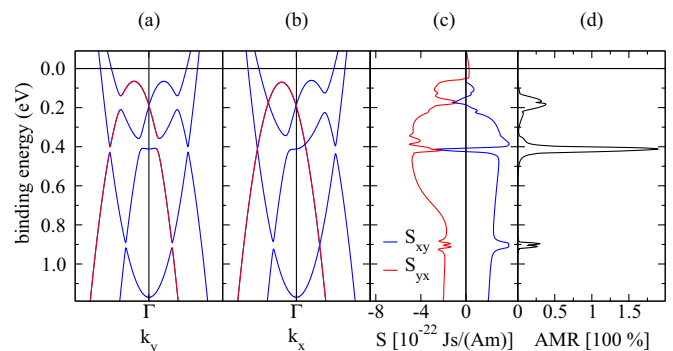

FIG. 5. (Left panel) Band structure of a 9-ML Ag(111) film on an Fe substrate with a Ag_2Bi surface alloy on top. Ag and Bi states are marked with circles and diamonds, respectively. Open and solid symbols indicate different spin orientations. Gray lines show Fe bands. (Right panels) Charge density of the QWS at the $\overline{\Gamma}$ point for two different energies. Gray regions indicate the Fe layers.

FIG. 6. Model band structure of the system along **k** (a) parallel and (b) perpendicular to the magnetization direction. (c) CISP for current along the y axis (S_{xy}) and current along the x axis (S_{yx}). (d) Calculated AMR ratio as a function of binding energy.

Close to the gaps the CISP differs strongly from the one of isolated Bi bands. The CISP depends on whether the current is in the y direction [S_{xy} in Fig. 6(c)] or in the x direction [S_{yx} in Fig. 6(c)], because for in-plane magnetization there is no rotational symmetry around the surface normal.

As noted above, the CISP leads to longitudinal changes in the magnetization, $\mathbf{M} + \delta\mathbf{M}$, depending on the current direction ($\pm x$). Since the resistivity depends only slightly on the absolute value of the magnetization, the induced asymmetry ($j_x - j_{-x}$) is small. On the other hand, the resistivity shows a pronounced dependence on the magnetization direction, as shown below. The AMR, defined as $2(\rho_{yy} - \rho_{xx})/(\rho_{yy} + \rho_{xx})$ with ρ_{yy} and ρ_{xx} as resistivities for current along the y and x axes, respectively, is shown in Fig. 6(d) as a function of the E_F position. Pronounced peaks in the AMR ratio in the range of 50%–150% arise when E_F is located in the vicinity of the points discussed above, where electronic bands for $\mathbf{k}$ parallel and perpendicular to the magnetization differ significantly. Away from the gaps the system behaves like a superposition of the isolated Bi and Ag bands with isotropic resistivities, leading to vanishing AMR. Thus, by tuning the position of E_F (by, e.g., alloying with Pb) it is possible to achieve gigantic values of the surface AMR.

For magnetization and current not perfectly perpendicular, the CISP can be used to exert a torque [12] on the magnetization, which rotates in-plane in response to the torque. In this case the combination of torque and AMR contributes to the quadratic term in the current-voltage characteristic, and alternatively the transverse voltage may be considered, since the AMR is accompanied by the planar Hall effect in this case. In fact, it has been recently shown [32] in ferromagnetic metallic layers with broken inversion symmetry and perpendicular anisotropy that, by combining the torque induced by the Rashba effect [15] and the anomalous Hall effect, one may quantify the torque from the second harmonic of the transverse voltage in the presence of an ac current. In contrast, our considerations apply to the case with in-plane anisotropy. In both cases, the quadratic response—which is most conveniently measured from the second harmonic accompanying an ac current—can be interpreted as manifestation of the $\mathbf{k}$ vs $-\mathbf{k}$ asymmetry in transport experiments.

IV. CONCLUSIONS

In summary, we reported the observation of particular electronic properties in film structures where exchange and spin-orbit interactions act on a comparable energy scale. The joint effect of the exchange and Rashba interactions, originating at the interface and at the surface of the film, respectively, is mediated by spin-polarized QWS and becomes spatially not limited to the film boundaries. The Rashba surface states and QWS acquire a particular $\mathbf{k}$ vs $-\mathbf{k}$ band asymmetry, due the concurrent breaking of time-reversal and structural-inversion symmetry. Spin-selective hybridization leads to asymmetric and spin-dependent band-gap openings, to an unequal number of states along the $\mathbf{k}$ and $-\mathbf{k}$ axes and to arc-formed constant energy contours. Model calculations show that this peculiar band-gap asymmetry can significantly influence spin-polarized transport properties.

APPENDIX A: EXPERIMENTAL GEOMETRY

Figures 7(a) and 7(b) display a sketch of the experimental geometries used for the angle-resolved photoemission measurements reported in Figs. 2 and 3. The shaded areas indicate the scattering plane of the experiment (light is p polarized). The two geometries correspond to different orientations between the Fe magnetization axis (Fe[001]) and the photoelectron collection plane.

Photoemission measurements were performed for the opposite sign of the magnetization (M^+, M^-) in both geometries [Figs. 7(c) and 7(d)]. The Fe layers were magnetized by a short magnetic pulse through a coil. Their remanent magnetic state was checked by magnetic linear dichroism of the Fe $3p$ core levels with 150 eV photons.
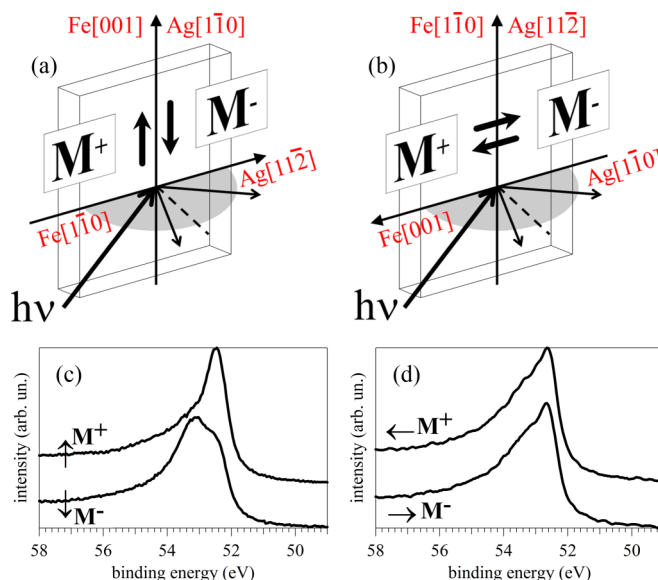

FIG. 7. Sketch of the experimental geometries used for the angle-resolved photoemission experiments. (a) The measured electrons are emitted in the plane containing the surface normal and the Fe[1$\bar{1}$0] axis. The photoemission measurement probes in reciprocal space the $\overline{M} - \overline{\Gamma} - \overline{M}$ direction of the Ag(111) films, which corresponds to the Ag[11$\bar{2}$] axis. (b) The measured electrons are emitted in the plane containing the surface normal and the Fe[001] axis. The photoemission measurement probe in reciprocal space the $\overline{K} - \overline{\Gamma} - \overline{K}$ direction of the Ag(111) films, which corresponds to the Ag[1$\bar{1}$0] axis. The electron wave vector is perpendicular to the magnetization axis in the first case and parallel to it in the second case. (c) and (d) Fe $3p$ photoemission spectra measured in the geometries of panels (a) and (b), respectively, for the opposite sign of the magnetization (M^+, M^-).
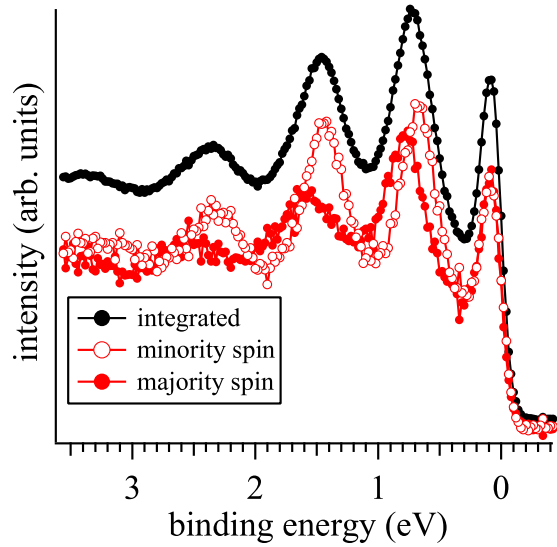
FIG. 8. Spin-resolved (solid red and open red symbols) and spin-integrated (solid black circles) photoemission spectra in normal emission for a 11 atomic layer Ag(111) film grown on Fe(110).

APPENDIX B: SPIN POLARIZATION OF THE Ag QWS

Spin and angle-resolved photoemission measurements of Ag(111) films on Fe(110) were taken on the U5UA beamline at the National Synchrotron Light Source of the Brookhaven National Laboratory (USA). As an example, Fig. 8 reports the spin-resolved and the corresponding spin-integrated photoemission spectra acquired in normal emission geometry with 50-eV photons for a 12-ML Ag(111) film grown on Fe(110). The spectra present a Shockley surface state near the Fermi level and several QWS at deeper energies. All photoemission peaks, except the surface state, display a spin polarization. In particular, the QWS appear to be spin-split and of predominantly minority-spin character. The exchange splitting as well as the relative weight of the two spin components depends on the binding energy.

These results can be rationalized by the DFT calculations shown in Fig. 5: In the energy region, where the Fe density of states (DOS) is predominantly of minority-spin d character, the minority-spin Ag s,p states are reflected strongly at the interface and remain better confined within the Ag layers. At this energy the Fe majority-spin electrons are more (s,p) type with a lower DOS and allow for a deeper penetration of the Ag QWS into the underlying film. The size of the exchange splitting of the QWS depends on the localization in the Ag film. States that extend more towards the interface to Fe (e.g., at 2 eV binding energy) show a stronger splitting than QWS that are localized in the middle of the film (e.g., at 1.2 eV binding energy; see Fig. 5).

APPENDIX C: ASYMMETRY IN CONSTANT ENERGY CUTS OF THE BAND STRUCTURE

The formation of band gaps due to spin-selective hybridization between QWS and Rashba surface states produces an asymmetry of the band structure, which can be observed in the angle-resolved photoemission data presented in the form of
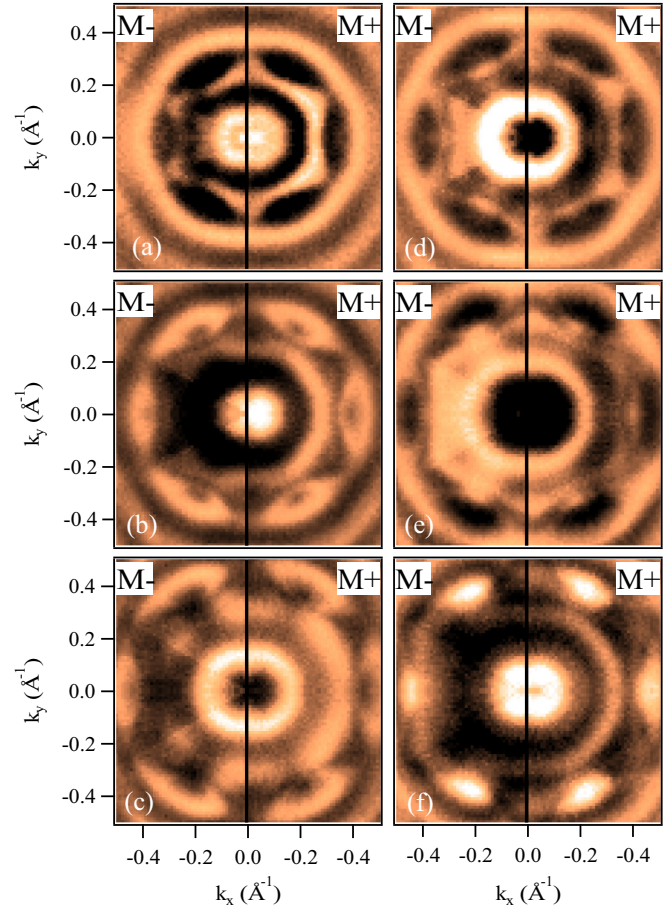

FIG. 9. Constant energy cuts for a $Ag_2Bi/11$ ML Ag/Fe(110) film, taken at binding energies (a) 0.34, (b) 0.70, (c) 0.92, (d) 1.12, (e) 1.28, and (f) 1.42 eV. The photon energy is 50 eV. The magnetization is aligned along the vertical axis.

constant energy cuts. Similarly to Fig. 4, in Fig. 9 we display constant energy cuts measured for a few binding energies, in the proximity of other band gaps. The left and right sides of each panel correspond to magnetization M^- and M^+. Several constant energy QWS contours present an open arc form.

APPENDIX D: MODEL HAMILTONIAN

To simulate transport properties, we tried to capture the essential properties of the electronic structure by a (4×4) model Hamiltonian:

$$H_0(\mathbf{k}) = H_{Bi}(\mathbf{k}) + H_{Ag,1}(\mathbf{k}) + H_{Ag,2}(\mathbf{k}) + H_{hyb,1} + H_{hyb,2}.$$

$$(D1)$$

Here,

$$H_{Bi}(\mathbf{k}) = \frac{(\hbar k)^2}{2m_{Bi}} + \alpha(\mathbf{z} \times \mathbf{k}) \cdot \boldsymbol{\sigma} + \Delta_{Bi} \quad (D2)$$

$$\text{and} \quad H_{Ag,j}(\mathbf{k}) = \frac{(\hbar k)^2}{2m_{Ag,j}} + \Delta_{Ag,j} \quad (D3)$$

describe the isolated Bi bands and two isolated minority-spin QWS, respectively, where kinetic energies are parametrized by masses m_{Bi} and $m_{Ag,j}$, α is the Rashba parameter, and $\boldsymbol{\sigma}$ is

the vector of Pauli spin matrices. For magnetization in the x direction, the hybridization of the jth QWS with the Bi bands is given by

$$H_{\text{hyb},j} = \frac{h_j}{\sqrt{2}} |\text{Ag},j\rangle [\langle \text{Bi} \uparrow | + \langle \text{Bi} \downarrow |] + \text{H.c.} \qquad (D4)$$

The model parameters $\hbar^2/(2m_{\text{Bi}}) = -35\,\text{eV bohr}^2$, $\alpha = 4.2\,\text{eV bohr}$, $\Delta_{\text{Bi}} = -0.196\,\text{eV}$, $\hbar^2/(2m_{\text{Ag},1}) = 17\,\text{eV bohr}^2$, $\Delta_{\text{Ag},1} = -0.4\,\text{eV}$, $\hbar^2/(2m_{\text{Ag},2}) = 30\,\text{eV bohr}^2$, and $\Delta_{\text{Ag},2} = -1.17\,\text{eV}$ for the Bi bands and the topmost occupied minority-spin QWS were determined from the DFT band structure shown in Fig. 5. We chose $h_1 = 0.05\,\text{eV}$ and $h_2 = 0.02\,\text{eV}$, reproducing typical hybridization gaps encountered in this system.

APPENDIX E: DISSIPATIONLESS TRANSPORT AT SINGULAR POINTS

Of particular importance for the transport properties are points in the band structure at which the hybridization between the QWS and Rashba bands depends on the direction in **k** space. One of such points, which is doubly degenerate due to the accidental crossing of the QWS and Rashba bands of opposite spin character, can be seen at 0.4 eV at positive k_x in Fig. 6(b). The constant energy cuts and the band surfaces around such a point are presented in Figs. 10(a) and 10(b).

Assuming that the Fermi energy cuts through the point of exact degeneracy and for simplicity focusing only on the region around the $\overline{\Gamma}$ point, we realize that the Fermi surface consists of a single point in this case, since for other directions in **k** space the hybridization between the quantum well state and the Rashba band occurs. This asymmetry is due to the spin-momentum locking of the spin-orbit split states, which opens a gap everywhere in the spectrum, except for the momentum
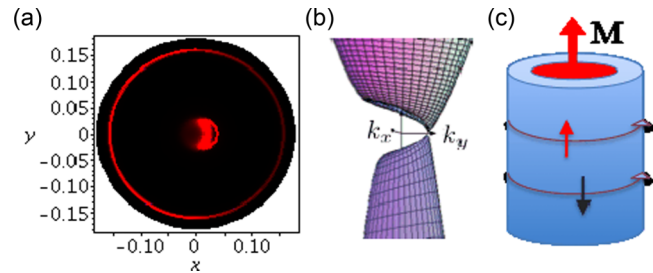

FIG. 10. (a) Constant energy cut through the band stucture shown in Fig. 6 of the main text at 0.4 eV. Two arclike features result from crossings of bands of opposite spin. (b) Band surface of the inner feature shown in (a). Energies 0.4 ± 0.1 eV are shown on the vertical axis. (c) Schematic presentation of the transport arising from the state at the touching point of this band surface in a cylinder geometry. **M** is the magnetic field from the Fe film.

direction where the spins are exactly parallel but opposite in sign. Although different in dimension and origin, the resulting band structure in Fig. 10(b) shows similarities to the one found in Weyl semimetals [33].

One can imagine a Gedanken experiment, in which the surface of the studied system is rolled into a cylinder such that the magnetization of the Fe(110) film [displayed in red in Fig. 10(c)] coincides with the cylinder axis. In this case, the two states at 0.4 eV, having opposite spin, will circumference the surface of the cylinder without possibility of back-scattering. In a sense, this would be analogous to the situation suggested to occur in two-dimensional quantum anomalous Hall insulators, for which the quantization of transverse conductance would lead to propagation of edge states which break the time-reversal symmetry. A similar scenario was suggested to occur in the metallic surface states of topological insulators exposed to an in-plane magnetic field [34].

[1] M. Z. Hasan and C. L. Kane, Rev. Mod. Phys. **82**, 3045 (2010).

[2] J.-i. Inoue, G. E. W. Bauer, and L. W. Molenkamp, Phys. Rev. B **67**, 033104 (2003).

[3] S. Datta and B. Das, Appl. Phys. Lett. **56**, 665 (1990).

[4] Y. A. Bychkov and E. I. Rashba, JETP Lett. **39**, 78 (1984).

[5] E. I. Rashba and Y. A. Bychkov, J. Phys. C **17**, 6039 (1984).

[6] X. C. Zhang, A. Pfeuffer-Jeschke, K. Ortner, V. Hock, H. Buhmann, C. R. Becker, and G. Landwehr, Phys. Rev. B **63**, 245305 (2001).

[7] S. LaShell, B. A. McDougall, and E. Jensen, Phys. Rev. Lett. **77**, 3419 (1996).

[8] G. Nicolay, F. Reinert, S. Hüfner, and P. Blaha, Phys. Rev. B **65**, 033407 (2001).

[9] C. R. Ast, J. Henk, A. Ernst, L. Moreschini, M. C. Falub, D. Pacilé, P. Bruno, K. Kern, and M. Grioni, Phys. Rev. Lett. **98**, 186807 (2007).

[10] C.-Z. Chang, J. Zhang, X. Feng, J. Shen, Z. Zhang, M. Guo, K. Li, Y. Ou, P. Wei, L.-L. Wang, Z.-Q. Ji, Y. Feng, S. Ji, X. Chen, J. Jia, X. Dai, Z. Fang, S.-C. Zhang, K. He, Y. Wang, L. Lu, X.-C. Ma, and Q.-K. Xue, Science **340**, 167 (2013).

[11] A. Manchon and S. Zhang, Phys. Rev. B **78**, 212405 (2008).

[12] A. Manchon and S. Zhang, Phys. Rev. B **79**, 094422 (2009).

[13] A. Matos-Abiague and R. L. Rodríguez-Suárez, Phys. Rev. B **80**, 094424 (2009).

[14] K.-W. Kim, H.-W. Lee, K.-J. Lee, and M. D. Stiles, Phys. Rev. Lett. **111**, 216601 (2013).

[15] I. M. Miron, G. Gaudin, S. Auffret, B. Rodmacq, A. Schuhl, S. Pizzini, J. Vogel, and P. Gambardella, Nat. Mater. **9**, 230 (2010).

[16] I. Miron, K. Garello, G. Gaudin, P. J. Zermatten, M. V. Costache, S. Auffret, S. Bandiera, B. Rodmacq, A. Schuhl, and P. Gambardella, Nature (London) **476**, 189 (2010).

[17] A. Chernyshov, M. Overby, X. Liu, J. K. Furdyna, Y. Lyanda-Geller, and L. P. Rokhinson, Nature Phys. **5**, 656 (2009).

[18] K. Garello, I. M. Miron, C. O. Avci, F. Freimuth, Y. Mokrousov, S. Blügel, S. Auffret, O. Boulle, G. Gaudin, and P. Gambardella, Nature Nanotech. **8**, 587 (2013).

[19] O. Krupin, G. Bihlmayer, K. Starke, S. Gorovikov, J. E. Prieto, K. Döbrich, S. Blügel, and G. Kaindl, Phys. Rev. B **71**, 201403(R) (2005).

[20] P. Moras, G. Bihlmayer, P. M. Sheverdyaeva, S. K. Mahatha, M. Papagno, J. Sánchez-Barriga, O. Rader, L. Novinec, S. Gardonio, and C. Carbone, Phys. Rev. B **91**, 195410 (2015).

[21] M. Mulazzi, M. Hochstasser, J. Fujii, I. Vobornik, G. Rossi, and J. Henk, Europhys. Lett. **82**, 57001 (2008).

[22] J. P. Perdew, K. Burke, and M. Ernzerhof, Phys. Rev. Lett. **77**, 3865 (1996).

[23] E. Wimmer, H. Krakauer, M. Weinert, and A. J. Freeman, Phys. Rev. B **24**, 864 (1981).

[24] H. Krakauer, M. Posternak, and A. J. Freeman, Phys. Rev. B **19**, 1706 (1979).

[25] FLEUR [http://www.flapw.de/].

[26] G. Bihlmayer, S. Blügel, and E. V. Chulkov, Phys. Rev. B **75**, 195414 (2007).

[27] I. G. Baek, W. Kim, E. Vescovo, and H. Lee, Phys. Rev. B **74**, 113302 (2006).

[28] E. Frantzeskakis, S. Pons, H. Mirhosseini, J. Henk, C. R. Ast, and M. Grioni, Phys. Rev. Lett. **101**, 196805 (2008).

[29] K. He, T. Hirahara, T. Okuda, S. Hasegawa, A. Kakizaki, and I. Matsuda, Phys. Rev. Lett. **101**, 107604 (2008).

[30] K. He, Y. Takeichi, M. Ogawa, T. Okuda, P. Moras, D. Topwal, A. Harasawa, T. Hirahara, C. Carbone, A. Kakizaki, and I. Matsuda, Phys. Rev. Lett. **104**, 156805 (2010).

[31] V. M. Edelstein, Solid State Commun. **73**, 233 (1990).

[32] U. H. Pi, K. W. Kim, J. Y. Bae, S. C. Lee, Y. J. Cho, K. S. Kim, and S. Seo, Appl. Phys. Lett. **97**, 162507 (2010).

[33] S.-M. Huang, S.-Y. Xu, I. Belopolski, C.-C. Lee, G. Chang, B. Wang, N. Alidoust, G. Bian, M. Neupane, C. Zhang, S. Jia, A. Bansil, H. Lin, and M. Z. Hasan, Nature Comm. **6**, 7373 (2015).

[34] A. M. Essin, J. E. Moore, and D. Vanderbilt, Phys. Rev. Lett. **102**, 146805 (2009).